Transportation Geotechnics 31 (2021) 100634

Contents lists available at ScienceDirect

Transportation Geotechnics

journal homepage: www.elsevier.com/locate/trgeo

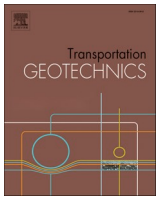

Evaluation of the effect of surcharge on the behavior of geosynthetic-reinforced soil walls

Raquel Mariano Linhares [a,*], Seyed Hamed Mirmoradi [b], Mauricio Ehrlich [b]

[a] Dept. of Engineering, ABI, Federal University of Lavras, Caixa Postal 3037, 37200-900 Lavras, MG, Brazil
[b] Dept. of Civil Engineering, COPPE, Federal University of Rio de Janeiro, RJ 21945-970, Brazil

ARTICLE INFO

Keywords:
Geosynthetic-reinforced soil (GRS) walls
Physical modelling
Numerical analysis
Surcharge width

ABSTRACT

In the current paper, using experimental studies and numerical analyses, the effect of surcharge width on the behavior of geosynthetic-reinforced soil (GRS) walls is evaluated under working stress conditions. Experimental tests were performed at the Geotechnical Laboratory of COPPE/UFRJ, using block and wrapped-face walls. Four well-instrumented GRS walls were examined considering different facing type and surcharge width. The numerical analysis of GRS walls was carried out using the two-dimensional computer program PLAXIS. Parametric studies were carried out with different combinations of surcharge width, wall height, compaction induced stresses (CIS) and face inclination. The results indicate the effect of the surcharge width in combination with other investigated factors on the magnitude and the position of the maximum reinforcement load and the lateral facing displacement of GRS walls.

Introduction

There are several benefits regarding the use of Mechanically Stabilized Earth (MSE) Walls in comparison with other conventional retaining structures, such as: lower prices, higher flexibility, better aesthetics, and the ability to reduce "bridge bumps" caused by differential settlements in pile supported abutments (e.g., [47,36,4,43,37,24,2]).

Some factors considerably influence the reinforcement tensile stresses, the lateral and vertical displacements, the shape and location of potencial failure surface and have already been studied, such as the relative soil-reinforcement stiffness index (Si), the soil type, plasticity and resistance parameters, pore water pressures, the face stiffness, the toe movement restriction and the combination of some of these factors [42,45,14,6,18,19,20,23,44,12,21,30,46,32,39]. Some other controlling factors, like the wall height, the compaction-induced stress (CIS) and the wall facing batter (ω) have also been studied, most of them in detached approaches or combined with a single surcharge applied at the total top surface area [22,14,16,38,40,11,13,41,27,34,8,3].

On the other hand, some works have been conducted with partial surcharges, analyzing its width and position, detached from other factors, or combined with the toe restriction, reinforcement stiffness and spacing. For clarity, are herein included the ones considering spread foundations and tiered configuration as surcharge loading, and GRS bridge abutments. The T_{max} position and value may be dependent on toe conditions, surcharge width and position, and is located below the centerline of surcharge width [48,5,2,33]. Also, the closer to facing is the surcharge, the greater the lateral earth pressures at back of the facing [5]. In addition, the surcharge position, in association with reinforcement stiffness, can also modify the failure mechanism and the potencial failure surface shape [16,38]. Partial surcharges, such as isolated footings, induce reinforcements strains at an exponential decreasing rate with depth, and can cause rotation of principal stresses, mobilizing reinforcement resistance in directions different from those considered in design [48].

The main contribution of this paper is the evaluation of the combined effect of surcharge width with wall height, CIS and wall facing batter on the GRS walls performance. First, the measurements from four well instrumented large-scale GRS walls constructed with different facing types and loaded with different surcharge widths are presented. Three of them had precast concrete block face and each one was submitted to a different surcharge width; the last one was a wrapped-face wall and was submitted to total surface surcharge. Following the physical modelling, a parametric study was carried out using the two-dimensional finite element program PLAXIS (ver 8.2) [9] in order to better understand the effect of surcharge width in combination with the wall height, compaction-induced stress (CIS) and facing inclination.

* Corresponding author.
E-mail addresses: raquel.linhares@ufla.br (R.M. Linhares), shm@ufrj.br (S.H. Mirmoradi), me@coc.ufrj.br (M. Ehrlich).

https://doi.org/10.1016/j.trgeo.2021.100634
Received 15 December 2020; Received in revised form 24 June 2021; Accepted 28 July 2021
Available online 31 July 2021

Noteworthy, the numerical analyses were carried out considering the wrapped-facing, only. This was performed to prevent the down-drag effect, which may occur close to structural facing element. The wrapped-face provides less complex numerical analyses and highlights the effect of other factors under consideration on GRSW behavior. Therefore, the numerical analysis was performed not to simulate the physical model tests precisely, but to separately evaluate the surcharge effects under the conditions similar to, but not exactly the same as, the physical model tests.

Physical modelling

Material used and construction sequence

The large-scale physical models of GRSW were constructed inside a "u-shaped" concrete box with dimensions of 2.00 m × 3.00 m × 1.50 m (width × length × height). The backfill soil was a crushed quartz with fabricated particle size distribution. The walls were 1.2 m high composed by six 0.20 m thick layers of soil, each one compacted dry for 10 min with a light vibrating plate (Dynapac LF 81), inducing an 8.0 kPa compaction stress and a 71% relative density on backfill soil. The facing batter (ω) were all 5.7° from the vertical (1:10 inclination). Three layers of flexible polyester geogrid were placed on top of the 1st, 3rd and 5th layers of soil (elevations 0.20, 0.60 and 1.00 m, respectively). The tensile stiffness modulus of the reinforcement, J_r, of 917 kN/m was determined based on the mechanical properties provided by the company. The length and vertical spacing of the geogrid were 2.3 m and 0.4 m, respectively.

A lubricated zone, made of rubber and silicon-based grease, was placed below the first layer of backfill soil, to move away the failure surface. As shown in Fig. 1, this model may represent the upper part of a 3.6 m high prototype, assuming a planar potential failure surface. Furthermore, to reduce the effect of lateral friction at the interface of the backfill soil and the concrete wall, PVC sheets were installed in the walls that composed the U-shaped concrete box of the model. In addition, a thin layer of Teflon grease covered by plastic sheets was used to assure plane-strain conditions during testing. Table 1 provides the material properties of the physical models. Backfill soil parameters determined by plane-strain test were presented by Ehrlich and Mirmoradi [12].

Following construction, the walls were submitted to surcharges from 0 to 100 kPa in stages of 20 kPa each, through a set of polymer airbags 60 cm wide placed under a reaction system made of wooden and steel beams fixed to the reinforced concrete floor. This arrangement allowed the authors to vary the imposed surcharge total widths by inflating one, two or all the polymer airbags. A model wall with precast block face can be seen in Fig. 2.

Three precast concrete block face walls were constructed and submitted to three different surcharge widths: 60 cm (q60), 120 cm (q120) and at total crest surface (q-total). Besides, the results of a wrapped-face wall submitted to a surcharge at total crest surface is presented. Of note, the measured values of the wrapped-face wall were presented by Mirmoradi et al. [35] and used for the validation of the numerical modelling. A cross sectional of the wall, instrumentation and surcharges is shown in Fig. 3. Table 2 shows a summary of physical model tests presented in the current paper.

Table 1
Material properties (physical models).

Property	Value
Precast block (face)	
Block weight (kg)	29
Dimensions (m)	0.2 × 0.4 x 0.4
Reinforcement (Geogrid)	
Tensile resistance (primary/secondary) (kN/m)	55/25
Tensile stiffness modulus, J_r (kN/m)	917
Length (m)	2.30
Backfill soil	
PI (%)	0
Gs	2.644
e_{max}	0.709
e_{min}	0.395
D_{50} (mm)	0.25
Cc	1
Cu	8.9
Unit weight, γ (kN/m^3)	19.00
Cohesion, c (kPa)	0
Friction angle, Φ (°)	50.0

Instrumentation

The walls were instrumented to monitor the values of the reinforcement load and horizontal facing displacement. Reinforcement

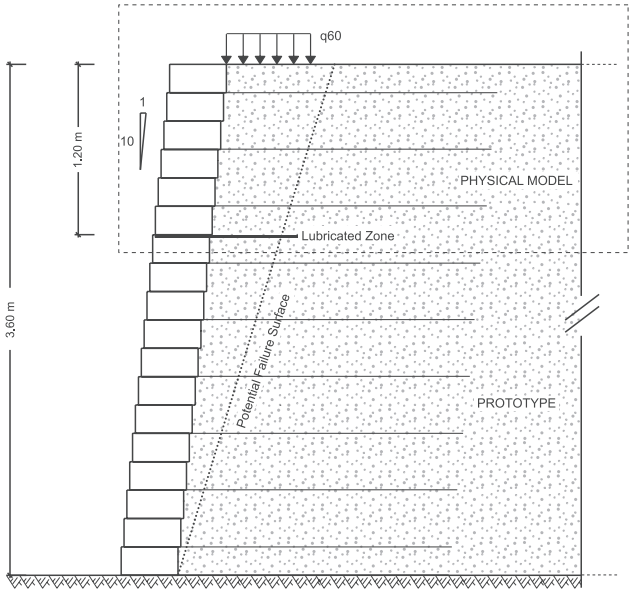

Fig. 1. Physical model height and prototype theoretical height due to lubricated zone.

Fig. 2. Physical mode built with precast block face.

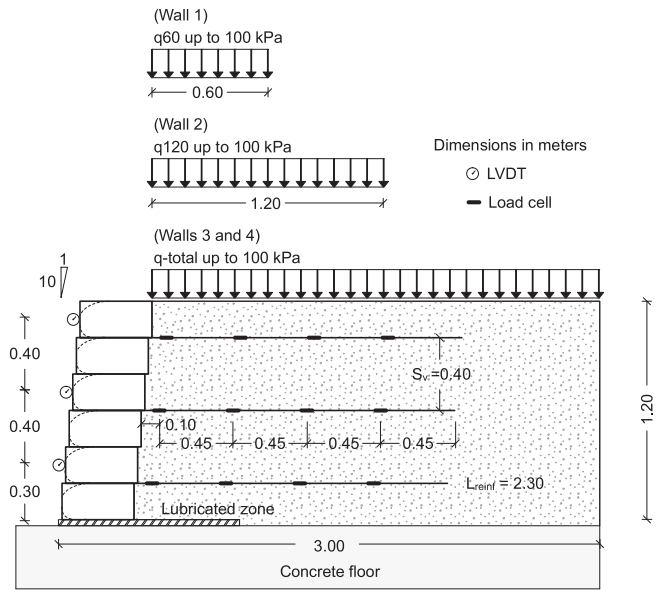

Fig. 3. Details of physical model instrumentation and surcharge widths.

Table 2
Physical models summary.

Face	Surcharge applied	Model name
Block Face	q60	Wall 1
Block Face	q120	Wall 2
Block Face	q-total	Wall 3
Wrapped-Face	q-total	Wall 4

loads were monitored using the load cells installed at four points along the reinforcement (two load cells in each point). Metal bars were used to link the load cells to the geogrids. The metal bars bundled the entire width of the geogrid reinforcement located in the central zone of the wall. The horizontal displacements of the wall face were monitored through LVDTs (Linear Variable Differential Transducers). The horizontal facing displacements were measured at the following elevations: 0.3 m (2nd layer), 0.7 m (4th layer), and 1.1 m (6th layer) (see Fig. 2).

Results of physical models

In this section, the reinforcement tensile stress (T) and lateral displacements (Δx) obtained from physical model instrumentation are analyzed. Fig. 4a shows the evolution of the summation of maximum reinforcement tensile stresses (ΣT_{max}) with surcharge. The summation of reinforcement tensile stresses along all reinforcement layers (ΣT) at end of construction (EOC) and end of loading (EOL) are shown in Fig. 4b.

Comparing both walls submitted to q-total, ΣT_{max} at EOC is higher in Wall 3 than Wall 4. This is due to construction process of Wall 4, which was laterally restricted with wood planks and steel beams up to the EOC [25,35]. At the EOC, the lateral restriction was taken out and therefore reinforcement tensile stress could be fully mobilized. By consequence, the difference between Walls 3 and 4 reduced with surcharge application and similar values of ΣT_{max} were obtained, irrespective of facing type. This agrees with the discussion presented by Ehrlich and Mirmoradi [12] and Mirmoradi and Ehrlich [28]. Regarding facing effect on RSWs performance, they elaborated that what control the reinforcement load is not facing stiffness only, but the combined effect of facing stiffness and toe restraint. Fig. 4a also shows a nonlinear behavior at the initial steps of surcharge loading due to the compaction effect.

Additionally, it is possible to see that Wall 1 presented the smallest values of ΣT_{max} observed in block face walls during surcharge application, with differences up to 20% in relation to Wall 3, which is corroborated by Mirmoradi and Ehrlich [33]. Additionally, Wall 2 and Wall 3 presented almost the same values of ΣT_{max} (maximum difference of 7% at EOL), indicating there is a maximum surcharge width that influences the reinforcement loads. One can relate the surcharge width with the wall height (H) and the estimated active (L_{act}) and passive zones surfaces at top of the wall. By Coulomb Method, $L_{act} = H.[\tan(45- (\omega + \Phi)/2)-\tan(\omega)]$. For $\Phi = 50^{\circ}$ and $\omega = 5.7^{\circ}$, $L_{act} = 0.21H$. Thus, trespassing 0.21H, an increment in surcharge width will not affect ΣT_{max} values. The surcharge widths herein, compared to the prototype height H, are 0.17H (Wall 1, q60), 0.34H (Wall 2, q120) and 0.69H (Walls 3 and 4, q-total), which confirms the arguments discussed.

Fig. 4b displays that, when all surcharges are located close to facing, q120 and q-total mobilized more intensively load cells further from facing than q60. It is important to notice that the surcharge width plays a combined role with the surcharge position, as discussed by Ambauen et al. [5] and Mirmoradi and Ehrlich [33]. As there were only four pair of load cells with fixed positions in all reinforcement layers, it could be complex to understand the magnitude of surcharge width influence in T distribution. To ease this interpretation, the area below each curve at EOL (total T) and its equivalent center of gravity were calculated, being: 6.34 kN and 0.49 m (Wall 1), 8.65 kN and 0.59 m (Wall 2), 9.27 kN and 0.58 m (Wall 3) and 8.38 kN and 0.57 m (Wall 4). Notable, q60 led to the smaller value of area of the reinforcement load curves and equivalent center of gravity. The other surcharge widths all led to similar values, corroborating the active zone discussion. These results also indicate a more pronounced mobilization of reinforcements below surcharges center line, in accordance with Ambauen et al. [5] and Mirmoradi and Ehrlich [33].

Fig. 5 shows the individual values of maximum reinforcement loads (T_{max}) with respective depths at EOC and EOL. All three walls with precast block facing (Walls 1, 2 and 3) presented similar T_{max} values and distribution with depth at EOC, with lower values at top and greater

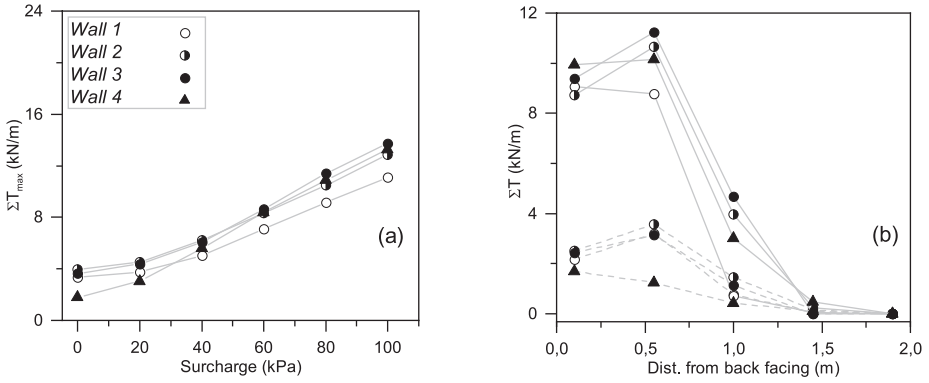

Fig. 4. Reinforcement tensile stresses for all walls: (a) ΣT_{max} during surcharge, (b) ΣT at End of Construction (dashed lines) and End of Loading (solid lines).

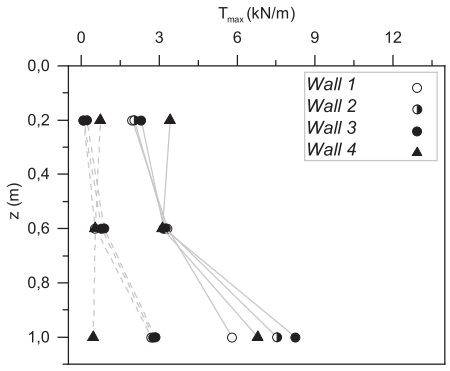

Fig. 5. T_{max} versus depth (z), at End of Construction (dashed lines) and End of Loading (solid lines) for all walls.

values at the bottom. On the other hand, Wall 4 presented opposite behavior at EOC, once again evidencing the construction process interference. At EOL, the T_{max} increment at Wall 4 bottom was more preeminent than at the top, reversing the T_{max} distribution shape with depth (difference from top to bottom evolved from −38.4% at EOC to +99.7% at EOL). The walls with precast block facing loaded with different surcharges still presented similar T_{max} distribution shape with depth (differences from top to bottom varying from 194.9% to 268.3%, all three cases being much higher than wrapped-face). Of note, these results should not be generalized for all walls. It depends on several factors such as soil type, facing and reinforcement stiffness, wall height, external load, etc.

Both T_{max} values at the wall top and bottom were higher, the wider the surcharge applied, indicating a direct relation between surcharge width and tension mobilization in reinforcements. It is important to emphasize that, even though the face type might influence T_{max} distribution shape with depth, ΣT_{max} values were similar for both cases loaded with total surface surcharge, as discussed by Ehrlich and Mirmoradi [12].

As stated earlier, the lateral displacements (Δx) were measured in three elevations at the walls facing (displacement profile), and they are shown for EOL in Fig. 6a. The Δx average value for each profile (Δx_{ave}) was then calculated for different surcharge levels and can be seen in Fig. 6b. Wall 4 presented the greater displacement values and deformed more uniformly than the block face walls (difference between top and bottom displacement was less than 5%). Also, Wall 4 presented the largest Δx_{ave} during surcharge application, being ≈23% greater than Wall 3 at EOL. The difference observed in Δx_{ave} values at EOL between Walls 3 and 4 is due to a local face deformation on wrapped-face wall, that tends to create a bulged area owed to geogrid flexibility, which increases LVDT readings [7,12]. Noteworthy, although ΣT_{max} values tend to be the same irrespective of facing type, lateral displacements may diverge at any stage due to a local face deformation on wrapped-face wall [12,30].

Regarding the precast block face walls, one can easily observe that the wider the surcharge, the greater the lateral displacements at EOL; also, the more uniformly the face deform. On the other hand, the narrower the surcharge, the greater the difference between top and bottom deformation (46.8% difference for q60 and 13.7% for q-total), which may be due to q60 being totally inserted in the active zone. Comparing to q-total, the differences at EOL stage are up to 30.6% and 12.2% for q60 and q120, respectively, which supports the T_{max} analyses.

Numerical models

General approach and material properties

Plane-strain numerical modeling was performed for wrapped-face GRS walls using the two-dimensional finite element program PLAXIS [9]. The results from a physical model constructed at Geotechnical Laboratory of COPPE/UFRJ were used to validate the numerical modeling. Good agreement between the measured and calculated values were presented by Ehrlich and Mirmoradi [12], Mirmoradi and Ehrlich [26,27,29] and Mirmoradi et al. [35]. Parametric study was then carried out to better elaborate the combined effects of surcharge width with factors, such as wall height (H), compaction-induced stress (CIS) and wall facing batter (ω).

The reinforcement length and the model total length were 0.70 and 1.70 of H. The reinforcements were spaced by 0.40 m (2 soil layers). A soft soil zone (6x6 cm) was included on the free end of each reinforcement element in the numerical mesh to ensure zero axial load at the ends of all reinforcement layers [28,10,35[49]].

The walls construction procedures were a sequential activation phases of the 0.20 m thick soil layer, the plate element on facing and the reinforcement above the actual layer, interspersed with compaction phases, when it was due. The CIS was modelled as suggested by Mirmoradi and Ehrlich [29][50], by activating uniform surcharges distributed above and below each layer and deactivating them on the following construction phase (Type II). Following the end of construction, a distributed load up to 100 kPa was applied at the wall top surface. Of note, in the physical model test, the facing was laterally restricted up to the end of construction. In the numerical analyses, the wrapped-face wall was simulated employing two different lateral facing restriction procedures during construction: with and without lateral restriction up to the end of construction. The results of the numerical analyses indicated practically the same ΣT_{max} values at EOC after the release of the restricted face and during surcharge application.

The backfill soil constitutive model was Hardening Soil, a behavior based on the Duncan-Chang hyperbolic model, where the soil stiffness is dependent on the confinement. A cohesion value of 1 kPa was used to improve numerical stability. In addition, the dilatancy angle was not

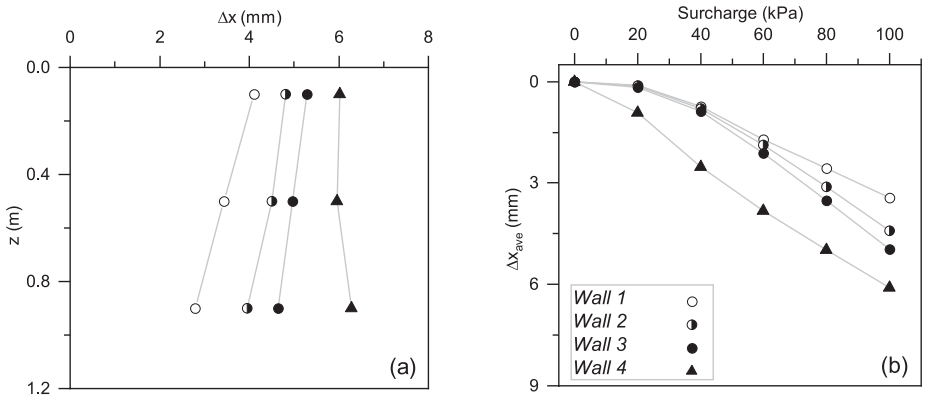

Fig. 6. Lateral displacements increment: (a) profiles at EOL; (b) average values during surcharge.

taken into consideration on this paper (Ψ = 0°), since under working stress conditions, this angle does not considerably influence ΣT_{max} values [31]. Nevertheless, the dilatancy angle might have a significant influence on wall performance near failure condition. Reinforcements were modeled as geogrids with elastic properties. Reader can be directed to Ehrlich and Mirmoradi [12] and Mirmoradi and Ehrlich [26,27,29] for more details. Table 3 provides the input parameters employed on the numerical analyses.

Variables in the parametric study

There were 4 variables in the parametric study which, combined, resulted in 21 different simulations. They were the wall height, H (3.6, 6.2 and 12.4 m), wall facing batter, ω (1:10, 1:6 and 1:3, approximately 5.7°, 9.5° and 18.4°, respectively) and CIS (without compaction (N/C), 60 and 120 kPa). Noteworthy, the effect of CIS was taken into consideration in isolation. This means that the modifications of backfill parameters due to compaction operation, such as dry density, friction angle and void ratio, were not taken into account in the performed analyses. Each one of these models were submitted to three different surcharge widths: 0.60, 1.20 m (q60 and q120, referred herein as partial surcharges) and at the total top' surface (q-total). Fig. 7 shows the numerical model geometry and parameters.

Numerical results

Influence of wall height

Fig. 8 illustrates normalized ΣT_{max} ($\Sigma T_{max}/(\gamma H^2 + 2.q.H)$) for different wall heights (3.6, 6.2 and 12.4 m), CIS = 0 kPa and ω = 5.7°, during application of surcharges with different widths (q60, q120 and q-total). The figure shows that, at EOC, the normalized ΣT_{max} is almost the same for all walls; the maximum difference was 8.2%, observed between H = 3.6 and H = 12.4 m. With the surcharge evolution, behavior disparities become more evident. At EOL, models submitted to q60 always presented the lower values of normalized ΣT_{max}, and the difference from those walls to the ones submitted to q120 varied from 13 to 29%, in all wall heights. For H = 3.6 m, there was indistinguishable variance between the ones surcharged with q120 and q-total (less than 2%), corroborating physical models results. In taller walls, those surcharged with q-total presented normalized ΣT_{max} values up to 26.6% greater from those surcharged with q120. The surcharge width in these cases would be approximately 0.17H and 0.33H (H = 3.6 m); 0.10H and 0.19H (H = 6.2 m) and 0.05H and 0.10*H* (H = 12.4 m), respectively, for

Table 3
Material properties (numerical models).

Property	Value
Backfill soil	
Unit weight, γ (kN/m^3)	21.00
Stiffness at 50% of failure, E_{50}^{ref} (kN/m^2)	42,500
Oedometric stiffness, E_{oed}^{ref} (kN/m^2)	31,770
Stiffness at failure, E_{ur}^{ref} (kN/m^2)	127,000
Power, m	0.50
Cohesion, c^{ref} (kPa)	1.00
Friction angle, Φ (°)	50.00
Dilatation angle, Ψ (°)	0.00
Poisson ration,ν	0.15
P^{ref} (kN/m^2)	100.00
At -rest earth lateral pressures coefficient, K_0	0.234
Failure ratio, Rf	0.700
Reinforcement	
Axial Stiffness, EA (kN/m)	600
Plate element (facing)	
Axial stiffness, EA (kN/m)	60.00
Bending stiffness, EI (kN·m^2/m)	1.00

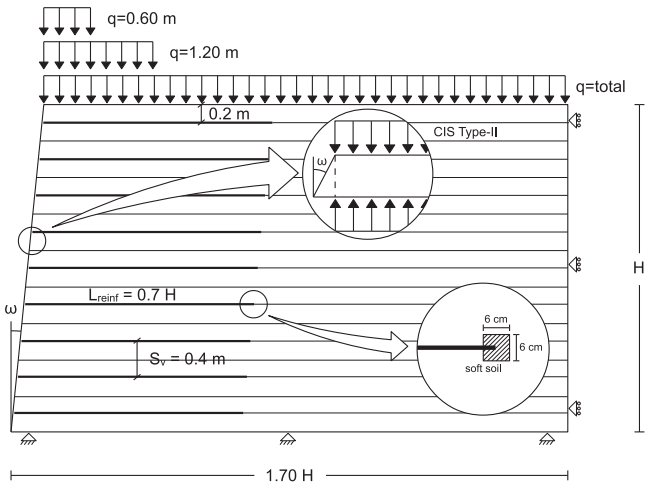

Fig. 7. Numerical model geometry and parameters.

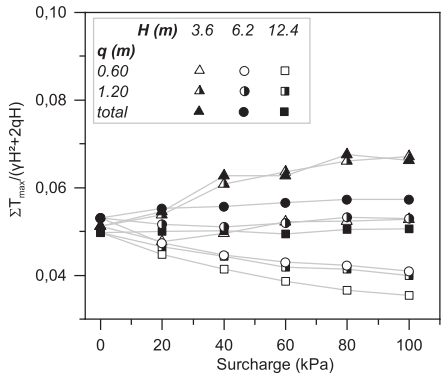

Fig. 8. Surcharge width and wall height combined effects on normalized ΣT_{max}.

q60 and q120. The performed analyses endorse the physical models' discussion; loading the 3.6 m high wall with q120 and q-total led to almost the same results and for H equal to 6.2 m and 12.4 m an increase difference on the results.

Fig. 9 presents normalized maximum reinforcement tensile stresses ($T_{max}/S_v.\gamma.H$) along normalized reinforcement depth (z/H) at EOC and at 50 kPa loading stage, for walls with three different heights (3.6, 6.2 and 12.4 m), CIS = 0 kPa and ω = 5.7°, submitted to surcharges with different widths (q60, q120 and q-total).

The figure shows that, at EOC, the distribution of normalized T_{max} with depth is similar, irrespective of the wall height. All reinforcement loads followed the line corresponding to the K_a-condition, which was expected due to low reinforcement stiffness and no compaction. When loaded with q-total, the curves remained fairly parallel to the EOC condition, from top to bottom. Regarding the partial surcharges (q60 and q120), T_{max} values are parallel to EOC condition at shallow depths, but the curves tend to detach from q-total curve in the lower reinforcement layers. The point where this detachment occurs is dependent on the surcharge width (approximately 2 times surcharge width) and seems to be independent of wall height. For the shortest wall (H = 3.6 m), there was indistinguishable variance between the ones surcharged with q120 and q-total, once again corroborating the indicative that increasing the surcharge width beyond 0.21H will not affect the T_{max} distribution as well as the normalized ΣT_{max} values.

Fig. 10 presents the normalized maximum reinforcement tensile stresses along normalized depth for two walls with identical ratios between H, surcharge width and magnitude: (i) H = 6.2 m, q60 at 50 kPa surcharge, and (ii) H = 12.4 m, q120 at 100 kPa surcharge. The

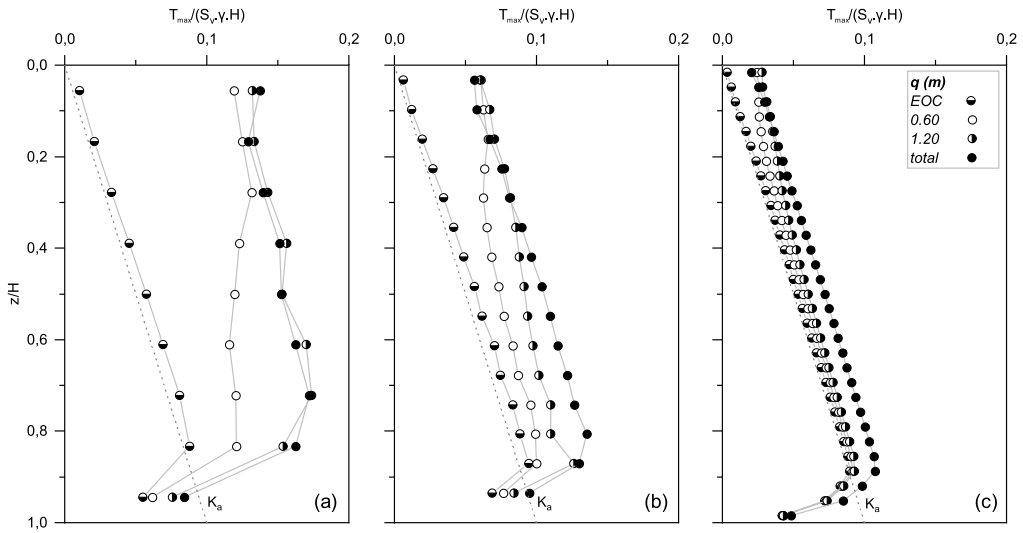

Fig. 9. Normalized T_{max} versus z/H, at EOC and at 50 kPa surcharge level for different wall heights (CIS = 0 kPa, ω = 5.7°): (a) H = 3.6 m, (b) H = 6.2 m and (c) H = 12.4 m.

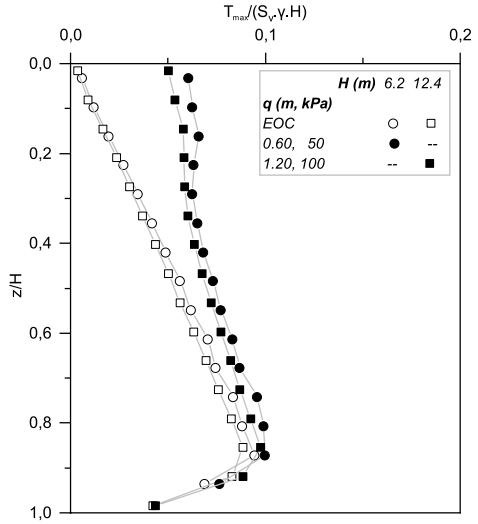

Fig. 10. Normalized T_{max} versus z/H for H = 6.2 m, q60 at 50 kPa surcharge level, and H = 12.4 m, q120 at 100 kPa surcharge level (CIS = 0 kPa, ω = 5.7°).

normalized tensions at EOC are also presented. The results are practically the same for the two normalized cases considered in this figure. This calls attention to the importance of the evaluation of the combined effect of wall height, surcharge width and magnitude on the behavior of reinforced soil structure.

Fig. 11 illustrates the normalized lateral (Δx/H) and vertical (Δy/H) maximum displacements of walls with different heights (3.6, 6.2 and 12.4 m), CIS = 0 kPa and ω = 5.7°, at EOC and EOL of surcharges with different widths (q60, q120 and q-total). At EOC, increasing H about 72% (3.6–6.2 m) augments Δx/H in 81% and Δy/H in 62.7%; increasing H another 100% (6.2–12.4 m) increases Δx/H in 81.5% and Δy/H in 74.3%. With loading evolution, the normalized displacement increments in comparison to EOC were up to 425% and 305% (H = 3.6 m), 170% and 147% (H = 6.2 m) and 70.8% and 67% (H = 12.4 m), for lateral and vertical displacements, respectively. This indicates that, when walls with different heights are loaded with the same surcharge width, the shorter tends to present greater proportional displacements.

However, the disparity between the normalized displacements observed in these cases tended to augment with H increase. Comparing q-total with q120 and q60, the variations were: 5.2% and 22.2% (H = 3.6 m), 11.1% and 33.8% (H = 6.2 m) and 20.6% and 32% (H = 12.4 m) for lateral displacements. Once again, the results indicate that there is a maximum surcharge width that influences walls behavior. The vertical displacements curves presented similar values to the horizontal ones. For H = 3.6 m, both normalized lateral and vertical maximum displacements are higher for q120 than q-total, but in small proportions (5.2 and 1.9%, respectively); this might be due to a major local displacement at wall top (local instability). With an H increase, the points related to q-total tend to surpass the ones related to q120,

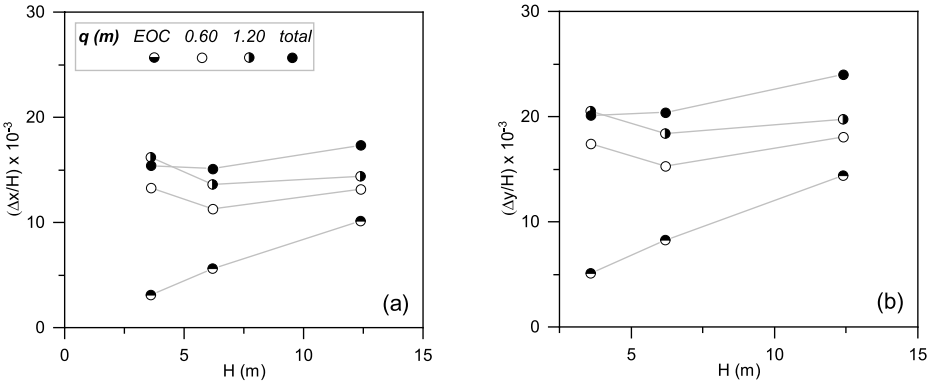

Fig. 11. Summary of (a) normalized lateral and (b) normalized vertical displacements, at EOC and EOL for different wall heights (CIS = 0 kPa, ω = 5.7°).

indicating that partial surcharges induce minor displacements in taller walls.

Influence of compaction-induced stresses (CIS)

Fig. 12 shows ΣT_{max} values for models submitted to different CIS (0, 60 and 120 kPa), H = 6.2 m and ω = 5.7°, loaded with different surcharge widths (q60, q120 and q-total). It is shown that at EOC, ΣT_{max} in compacted walls were 10% and 55% greater relatively to non-compacted wall, for CIS = 60 and 120 kPa, respectively. At EOL, these initial disparities had mostly vanished, and the ΣT_{max} was considerably dependent on the surcharge width. This illustrates that although the compaction effort increases ΣT_{max} up to the EOC, it reduces the reinforcement load gain with surcharge application. Additionally, it seems that the reinforcement load gain is strongly related to surcharge width, being greater the wider the surcharge. The results indicate that, when the surcharge overcomes the CIS, there is no practical difference of ΣT_{max} between walls with or without modelling of CIS.

Furthermore, in this figure is shown that, at EOL, the non-compacted wall presented the higher discrepancies of ΣT_{max} values between partial surcharges (30%). This difference decreased to 22% when the wall was compacted with 120 kPa. Also, at EOL, there was about 8% difference between q-total and q120 for the non-compacted wall. Increasing the compaction effort results in higher differences but seemed to reach a limit of 18% in both cases. That indicates narrow surcharges affects more non-compacted walls, and the widening of surcharge influence increases up to a limit with application of compaction effort.

Fig. 13 indicates the normalized lateral (Δx/H) and vertical (Δy/H) maximum displacements of walls submitted to different CIS (0, 60 and 120 kPa), H = 6.2 m and ω = 5.7°, at EOC and EOL of surcharges with different widths (q60, q120 and q-total). The figures show that the CIS leads to larger lateral and vertical maximum normalized displacements during construction. Compared to non-compacted wall, they were, respectively, 90% and 250% (lateral) and 41% and 110% (vertical) greater, for CIS = 60 and 120 kPa, respectively. From EOC to EOL, the Δx/H increased 102%, 143% and 170%, for q60, q120 and q-total, respectively, in non-compacted walls; for CIS = 120 kPa, the increments were 15%, 25% and 36%, respectively, evidencing that both lateral and vertical displacements evolution during surcharge application are at smaller rate when the backfill soil is compacted and submitted to narrow surcharges.

For q-total, backfill heave compaction (CIS = 120 kPa) in comparison to the no compaction condition led to a decrease in lateral displacements up to 134%. Although visually the offset between EOL points seems the same for all CIS, the higher the CIS, the lower the difference between the displacements observed. Comparing q-total with q60, the differences are up to 33% (N/C, lateral displacements) and 23.6% (CIS = 120 kPa, vertical displacements). These results indicate compacted GRSW tend to present a slightly more similar behavior under different surcharge widths.

The CIS modelling leads to larger lateral and vertical displacements during construction and reduce both lateral and vertical displacements evolution during surcharge application. This means that the CIS could be understood as a kind of preconsolidation of the reinforced soil mass (e.g., [15,13]). The current study calls attention to the combined effect of the surcharge width and CIS on the wall behavior.

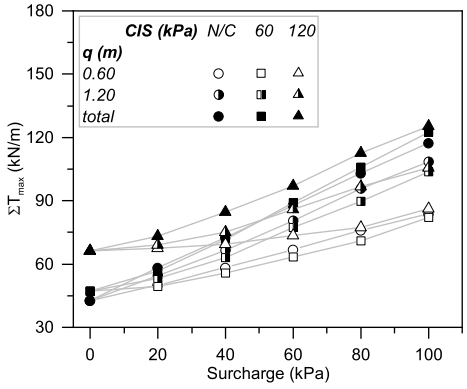

Fig. 12. Surcharge width and backfill soil compaction combined effects on ΣT_{max} (H = 6.2 m, ω = 5.7°).

Influence of facing batter angle

Fig. 14 compares ΣT_{max} values for walls with different facing batters (5.7°, 9.5° and 18.4°), H = 6.2 m and CIS = 0 kPa, loaded with different surcharge widths (q60, q120 and q-total). Fig. 14 It indicates that for a given surcharge condition, the walls with lower batters presented the higher ΣT_{max} at EOC and at EOL. The disparities of ΣT_{max} values between walls submitted to different surcharge widths are 8.2% and 40% (ω = 5.7°), 12% and 43% (ω = 9.5°) and 6.8% and 31% (ω = 18.4°), from q-total to q120 and q60, respectively.

Fig. 15 presents the normalized maximum reinforcement tensile stresses ($T_{max}/S_v.\gamma.H$) with normalized reinforcement depth (z/H) at EOC and at 50 kPa loading stage, for different wall facing batters (ω = 5.7°, 9.5° and 18.4°), H = 6.2 m and CIS = 0 kPa, submitted to surcharge with different widths (q60, q120 and q-total). The figure shows that at EOC and when loaded with q-total, the reinforcement loads curves for the near vertical wall (w = 5.7°), may be assumed as parallel ones. Nevertheless, with the increase of facing batter, those two curves (EOC and q-total) tend not to be parallel anymore, which is more pronounced for the models with ω = 18.4° (see Fig. 15c). This means that the combined effect of facing inclination and surcharge may control the shape of the distribution of T_{max} with depth.

When submitted to partial surcharges (q60 and q120), the T_{max} values tend detach from those of q-total curve and with depth become near to corresponding value of the EOC condition. Comparing the normalized T_{max} values calculated at EOC, for the second reinforcement layer near the top, the differences are as high as 415% and 453% (ω = 5.7°) and 508% and 486% (ω = 18.4°), for q60 and q120 respectively; as for the reinforcement layer near the bottom of the wall the differences are as low as 12% and 22% (ω = 5.7°) and 5% and 12% (ω = 18.4°), for q60 and q120, respectively. In other words, for a given surcharge conditions, the more inclined the face is, the more uniform distribution of T_{max} with depth is.

Vertical stress distribution with depth may be closely represented by triangular shape in vertical walls. Under this condition, the vertical stress has a direct relation with depth from the wall top. Vertical stress is also affected by facing inclination, being smaller at the bottom of the wall the more inclined the face is. Moreover, partial surcharges mostly affect the stress at the top of the wall, resulting in more constant distribution of vertical stress and therefore T_{max} with depth.

Fig. 16 shows the normalized lateral (Δx/H) and vertical (Δy/H) maximum displacements of walls with different facing batters (5.7°, 9.5° and 18.4°), H = 6.2 m and CIS = 0 kPa, at EOC and EOL of surcharges with different widths (q60, q120 and q-total). Those figures show that the steeper the wall face, the higher are the Δx/H and Δy/H values at EOC, which was expected. Comparing both partial surcharges (q60 and q120) at EOL, the discrepancies in Δx/H and Δy/H values were about 20% for all wall face batters, revealing that partial surcharge width increment did not play a combined role with the wall face batter. On the other hand, comparing the results for q60 and q-total, the differences in Δx/H values were about 34% (ω = 5.7°) 29% (ω = 9.5°) and 28% (ω = 18.4°), indicating there is, indeed, a combined effect of surcharge width and wall face batter in calculated displacements, the displacements being greater the steeper the walls. This effect is pronounced when the surcharge width varies from partial to total. For Δy/H values, the percentage differences were 1% lower, in all cases.

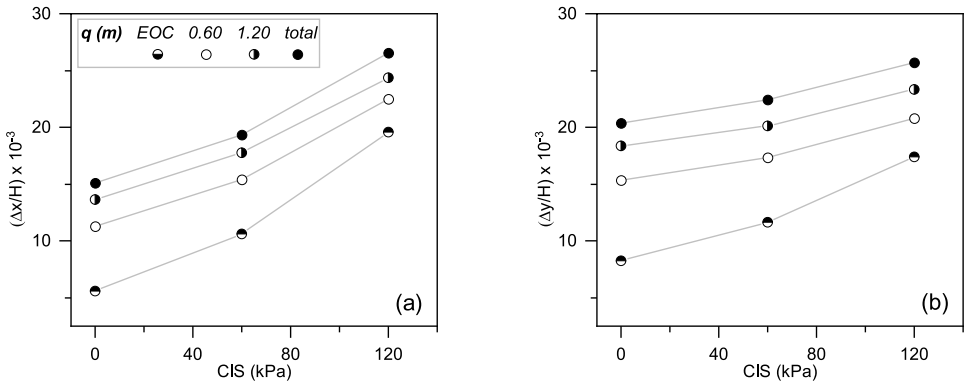

Fig. 13. Summary of (a) normalized lateral and (b) normalized vertical displacements, at EOC and EOL for CIS (H = 6.2 m, ω = 5.7°).

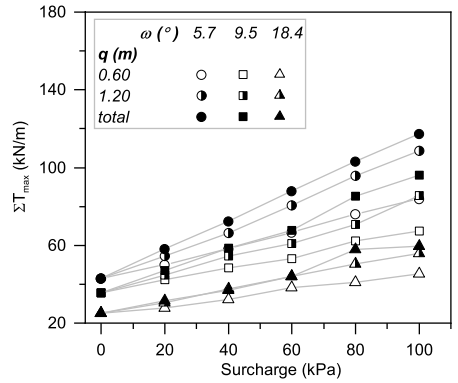

Fig. 14. Surcharge width and wall facing batter combined effects on T_{max} (H = 6.2 m, CIS = 0 kPa).

Conclusions

The current study experimentally and numerically assessed the effect of surcharge width on GRS walls performance. Four large-scale physical models were built, at COPPE/UFRJ facilities. Three of them had precast concrete block face and each one was submitted to a different surcharge width (60 cm, 120 cm and over the entire surface of the wall top); the last one was a wrapped-face wall and was submitted to total surface surcharge. Additionally, numerical analyses were carried out considering the combined effect of surcharge width with wall height, facing inclination and compaction-induced stress.

The results of the physical and numerical studies suggest there is a maximum surcharge width (about 0.21H for Φ = 50°and ω = 5.7°) that can influence the reinforcement loads. Beyond that, increasing surcharge width may affect lateral displacements and the wall deformation profile at EOL, but may not interfere on T_{max} values. Of note, the AASHTO [1] simplified method for predicting the T_{max} values limits the average vertical pressure due to soil surcharge on the top of the reinforced soil mass up to a maximum width of 0.70H, which depending on surcharge conditions and reinforcement position may lead to conservative or non-conservative representation of the field condition.

The numerical study also indicates that backfill compaction anticipate movements during construction and increase the reinforcements loads, promoting a kind of prestress in the reinforced soil mass, reducing post construction movements. The greater is the compaction-induced stresses (CIS) the greater are ΣT_{max} and lateral and vertical displacements at EOC. For CIS = 120 kPa, in comparison to non-compacted walls it was observed an increase of the value of ΣT_{max} and lateral and vertical displacements of 55%, 250% and 110%, respectively. At EOL, the higher the CIS, both ΣT_{max} values and displacements evolution during

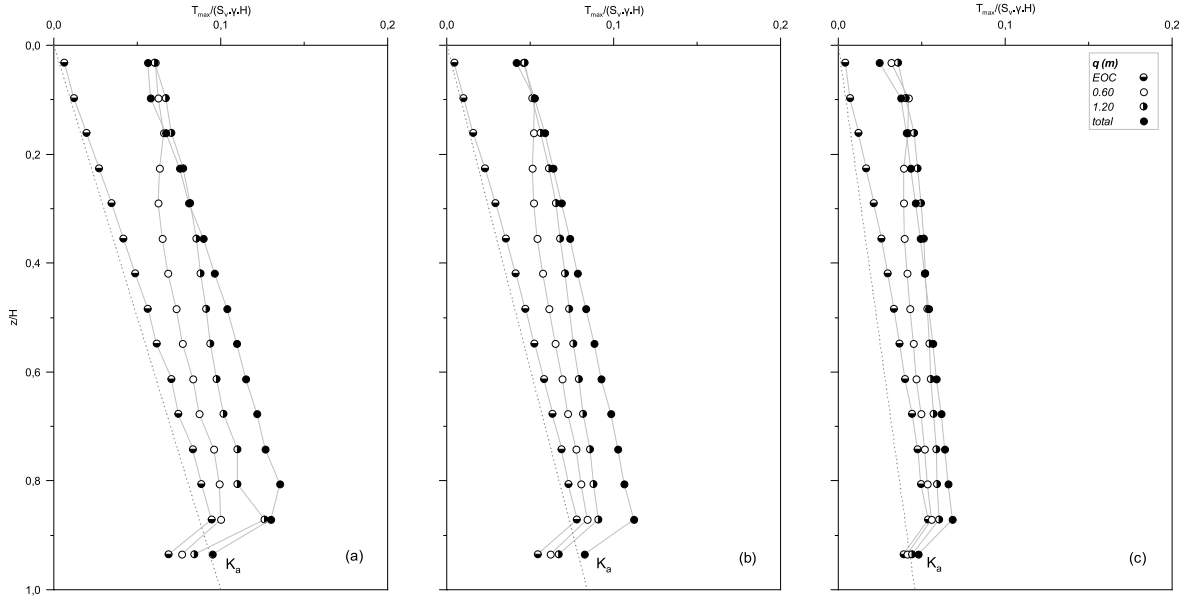

Fig. 15. Normalized T_{max} versus z/H, at the EOC and at 50 kPa surcharge level, for different surcharge widths and wall facing batter (H = 6.2 m, CIS = 0 kPa): (a) 5.7°; (b) 9.5° and (c) 18.4°.

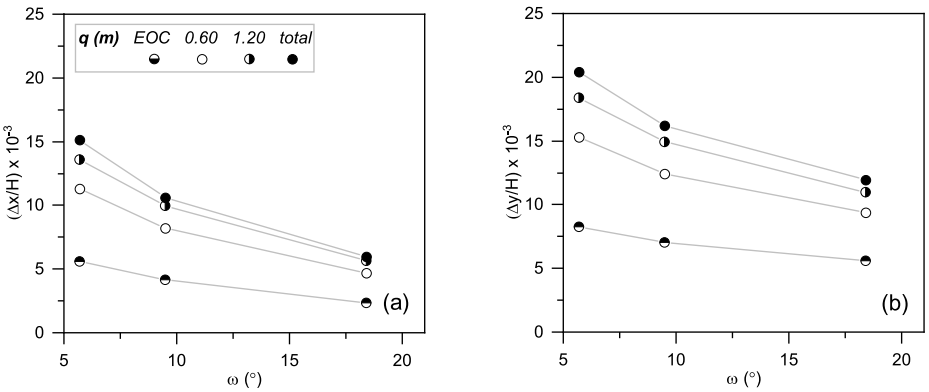

Fig. 16. Summary of (a) normalized lateral and (b) normalized vertical displacements, at EOC and EOL for different wall facing batter angles (H = 6.2 m; CIS = 0 kPa).

surcharge application are at smaller rate. This effect is more relevant the narrower the surcharge is.

The combined effect of facing inclination and surcharge width affects the T_{max} distribution with depth, the shape evolving from a triangular form to a rectangular one the more inclined the face is. This is valid for both partial and total surcharges, but the effect is more preeminent with the latter. This means T_{max} values become more uniform with reinforcement depth, and a better suited design is facilitated. Of note, in the current design methods this effect is not taken into consideration in the T_{max} calculation.

CRediT authorship contribution statement

Raquel Mariano Linhares: Conceptualization, Methodology, Software, Validation, Formal analysis, Writing – original draft, Visualization. **Seyed Hamed Mirmoradi:** Conceptualization, Methodology, Validation, Investigation, Writing – review & editing, Supervision. **Mauricio Ehrlich:** Conceptualization, Methodology, Validation, Investigation, Resources, Writing – review & editing, Supervision, Funding acquisition.

Declaration of Competing Interest

The authors declare that they have no known competing financial interests or personal relationships that could have appeared to influence the work reported in this paper.

Acknowledgements

The authors greatly appreciate the funding of this study by the Brazilian Research Council CNPq and the Coordenação de Aperfeiçoamento de Pessoal de Nível Superior - Brasil (CAPES).

References

[1] AASHTO. AASHTO LRFD bridge design specifications, 8th ed. Washington, D.C., USA: American Association of State Highway and Transportation Officials; 2017.
[2] Abu-Farsakh M, Ardah A, Voyiadjis G. 3D finite element analysis of the geosynthetic reinforced soil-integrated bridge system (GRS-IBS) under different loading conditions. Transp Geotech 2018. https://doi.org/10.1016/j.trgeo.2018.04.002.
[3] Abu-Farsakh MY, Ardah A, Voyiadjis GZ. Numerical parametric study to evaluate the performance of a Geosynthetic Reinforced Soil-Integrated Bridge System (GRS-IBS) under service loading. Transp Geotech 2019. https://doi.org/10.1016/j.trgeo.2019.04.001.
[4] Abu-Hejleh N, Wang T, Zornberg JG. Performance of geosynthetic-reinforced walls supporting bridge and approaching roadway structures. Adv Transp Geoenviron Syst Geosynthetics ASCE 2000:218–43.
[5] Ambauen S, Leshchinsky B, Xie Y, Rayamajhi D. Service state behavior of reinforced soil walls supporting spread footings – a parametric study using FE analysis. Geosynthetics Int 2015. https://doi.org/10.1680/jgein.15.00039.
[6] Bathurst RJ, Walters DL, Vlachopoulos NP, Burgess PG, Allen TM. Full scale testing of geosynthetic reinforced walls. Canadian Geotech J 2000;44:1484–90.
[7] Benjamim CVS, Bueno BS, Zornberg JG. Field monitoring evaluation of geotextile-reinforced soil-retaining walls. Geosynthetics Int 2007;14(2):100–18.
[8] Benmebarek S, Djabri M. FEM to investigate the effect of overlapping-reinforcement on the performance of back-to-back embankment bridge approaches under self-weight. Transp Geotech 2017. https://doi.org/10.1016/j.trgeo.2017.03.002.
[9] Brinkgreve RBJ, Vermeer PA. PLAXIS: finite element code for soil and rock analyses, version 8. Leiden, Netherlands: CRC Press; 2002.
[10] Damians IP, Bathurst RJ, Josa A, Lloret A. Numerical analysis of an instrumented steel-reinforced soil wall. Int J Geomech 2015;15(1). https://doi.org/10.1061/(ASCE)GM.1943-5622.0000394.
[11] Ehrlich M, Becker LDB. Reinforced soil wall measurements and predictions. In: Proceeding 9th int conf on geosynthetics, vol. CD-ROOM. Guarujá, SP, Brazil; 2010. p. 547–59.
[12] Ehrlich M, Mirmoradi SH. Evaluation of the effects of facing stiffness and toe resistance on the behavior of GRS walls. Geotext Geomembr 2013;40:28–36.
[13] Ehrlich M, Mirmoradi SH, Saramago RP. Evaluation of the effect of compaction on the behavior of geosynthetic-reinforced soil walls. Geotext Geomembr 2012;34:108–15.
[14] Ehrlich M, Mitchell JK. Working stress design method for reinforced soil walls. J Geotech Eng ASCE 1994;120(4):625–45.
[15] Ehrlich M, Mitchell JK. Working stress design method for reinforced soil walls–closure. J. Geotech. Eng. ASCE 1995;121(11):820–1.
[16] Gomes RC, Palmeira EM, Lanz D. Failure and deformation mechanisms in model reinforced walls subjected to different loading conditions. Geosynthetics Int 1994;1(1):45–65.
[18] Hatami K, Bathurst RJ. Development and verification of a numerical model for the analysis of geosynthetic-reinforced soil segmental walls under working stress conditions. Canadian Geotech J 2005;42:1066–85. https://doi.org/10.1139/T05-040.
[19] Hatami K, Bathurst RJ. Numerical model for reinforced soil segmental walls under surcharge loading. J Geotech Geoenviron Eng 2006;132(6):673–84.
[20] Huang B, Bathurst RJ, Hatami K, Allen TM. Influence of toe restraint on reinforced soil segmental walls. Canadian Geotech J 2010;47:885–904.
[21] Jacobs F, Ruiken A, Ziegler M. Investigation of kinematic behavior and earth pressure development of geogrid reinforced soil walls. Transp Geotechnics 2016. https://doi.org/10.1016/j.trgeo.2016.07.004.
[22] Leshchinsky D, Boedeker RH. Geosynthetic reinforced soil structures. J Geotech Eng 1989;115(10):1459–78.
[23] Leshchinsky D, Vahedifard F. Impact of toe resistance in reinforced masonry block walls: design dilemma. J Geotech Geoenviron Eng ASCE 2012;138(2):236–40.
[24] Liu H, Won MS. Long-term reinforcement load of geosynthetic-reinforced soil retaining walls. J Geotech Geoenviron Eng ASCE 2009;135(7):875–89.
[25] Mirmoradi SH. Evaluation of the behavior of reinforced soil walls under working stress conditions [Ph.D. thesis]. Rio de Janeiro, Brazil: COPPE/UFRJ; 2015. p. 340.
[26] Mirmoradi SH, Ehrlich M. Geosynthetic reinforced soil walls: experimental and numerical evaluation of the combined effects of facing stiffness and toe resistance on performance. In: Proceeding 10th int conf on geosynthetics. London: Ed. Int Society of Soil Mechanics Geotech Eng (ISSMGE); 2014a.
[27] Mirmoradi SH, Ehrlich M. Modeling of the compaction-induced stresses in numerical analyses of GRS walls. Int J Comput Methods 2014;11(2):1342002. https://doi.org/10.1142/S0219876213420024.
[28] Mirmoradi SH, Ehrlich M. Numerical evaluation of the behavior of grs walls with segmental block facing under working stress conditions. ASCE J Geotech Geoenviron Eng 2015;141(3):04014109.
[29] Mirmoradi SH, Ehrlich M. Modeling of the compaction-induced stress on reinforced soil walls. Geotext Geomembr 2015;43:82–8.
[30] Mirmoradi SH, Ehrlich M. Evaluation of the effect of toe restraint on GRS walls. Transp Geotechnics 2016;8:35–44.
[31] Mirmoradi SH, Ehrlich M. Closure to Numerical evaluation of the behavior of grs walls with segmental block facing under working stress conditions. ASCE J Geotech

Geoenviron Eng 2016;:07016002. https://doi.org/10.1061/(ASCE)GT.1943-5606.0001235.
[32] Mirmoradi SH, Ehrlich M. Effects of facing, reinforcement stiffness, toe resistance, and height on reinforced walls. Geotext Geomembr 2017;45(1):67–76.
[33] Mirmoradi SH, Ehrlich M. Experimental evaluation of the effects of surcharge width and location on geosynthetic-reinforced soil walls. Int J Phys Model Geotechnics 2019. https://doi.org/10.1680/jphmg.16.00074.
[34] Mirmoradi SH, Ehrlich M, Dieguez C. Evaluation of the combined effect of toe resistance and facing inclination on the behavior of GRS wall. Geotext Geomembr 2016;44:287–94.
[35] Mirmoradi SH, Ehrlich M, Chinchay P, Dieguez C. Evaluation of the combined effect of facing inclination and uniform surcharge on GRS walls. Geotext Geomembr 2019;47(5):103485. https://doi.org/10.1016/j.geotexmem.2019.103485.
[36] Mitchel JK, Villet WCB. Reinforcement of earth slopes and embankments. Washington, D.C.: Ed. Transportation Research Board National Research Council; 1987.
[37] Nicks JE, Adams MT, Ooi PSK, Stabile T. Geosynthetic reinforced soil performance testing – axial load deformation relationships. McLean, VA, USA: FHWA Research, Development and Technology, Report of the Federal Highway Administration (FHWA)- HRT-13-066; 2013.
[38] Palmeira EM, Gomes RC. Comparisons of predicted and observed failure mechanisms in model reinforced soil walls. Geosynthetics Int 1996;3(3):329–47.
[39] Rajagopal G, Thiyyakkandi S. Numerical evaluation of the performance of back-to-back MSE walls with hybrid select-marginal fill zones. Transp Geotechnics 2020. https://doi.org/10.1016/j.trgeo.2020.100445.
[40] Riccio MV, Ehrlich M. Performance of a block-faced geogrid wall using fine-grained tropical soils. In: Proceeding 17th int conf soil mech and geotech eng, vol. 2. Alexandria: Ed. Int Society Soil Mech Geotech Eng; 2009. p. 1877–80.
[41] Riccio M, Ehrlich M, Dias D. Field monitoring and analyses of the response of a block-faced geogrid wall using fine-grained tropical soils. Geotext Geomembr 2014;42:127–38.
[42] Rowe RK, Ho SK. 1993. Keynote lecture: a review of the behavior of reinforced soil walls. In: Ochiai H, Hayashi S, Otani J, editor. Proceeding int symp on earth reinforcement practice '93, vol. 2. Rotterdam, The Netherlands; 1993. p. 801–30.
[43] Skinner GD, Rowe KR. Design and behaviour of a geosynthetic reinforced retaining wall and bridge abutment on a yielding foundation. Geotext Geomembr 2005;23:234–60.
[44] Stuedlein AW, Allen TM, Holtz RD, Christopher BR. Assessment of reinforcement strains in very tall mechanically stabilized earth walls. J Geotech Geoenviron Eng ASCE 2012;138(3):345–56.
[45] Tatsuoka F. Keynote lecture: roles of facing rigidity in soil reinforcing. In: Ochiai H, Hayashi S, Otani J, editor. Proceeding int symp on earth reinforcement practice '93, vol. 2. Rotterdam, The Netherlands; 1993. p. 831–70.
[46] Vahedifard F, Mortezaei K, Leshchinsky BA, Leshchinsky D, Lu N. Role of suction stress on service state behavior of Geosynthetic-Reinforced Soil Structures. Transp Geotechnics 2016. https://doi.org/10.1016/j.trgeo.2016.02.002.
[47] Vidal H. The principles of reinforced earth. Highway Res Rec 1969;282:1–16.
[48] Yoo C, Kim SB. Performance of a two-tier geosynthetic reinforced segmental retaining wall under a surcharge load: Full-scale load test and 3D finite element analysis. Geotext Geomembr 2008;26:460–72.
[49] Nascimento G, Ehrlich M, Mirmoradi SH. Simulation of compaction-induced stress for the analysis of RS walls under surcharge loading. Geotextiles and Geomembranes 2020;48(4):532–8. https://doi.org/10.1016/j.geotexmem.2020.02.011.
[50] Mirmoradi SH, Ehrlich M. Numerical simulation of compaction-induced stress for the analysis of RS walls under working conditions. Geotextiles and Geomembranes 2018;46(3):354–65. https://doi.org/10.1016/j.geotexmem.2018.01.006.